Tribology Letters, Vol. 23, No. 1, July 2006 (© 2006)
DOI: 10.1007/s11249-006-9104-x

The friction properties of an ultrathin confined water film

M. Paliy[a,*], O.M. Braun[b,c] and S. Consta[a]

[a]*Department of Chemistry, University of Western Ontario, London, Ontario, N6A 5B7, Canada*
[b]*Institute of Physics, National Academy of Sciences of Ukraine, 03028, Kiev, Ukraine*
[c]*Centre for Chemical Physics, University of Western Ontario, London, Ontario, N6A 3K7, Canada*

Received 3 November 2005; accepted 13 July 2006; published online 5 August 2006

An ultrathin water film confined between two substrates in moving contact is studied using Langevin molecular dynamics with coordinate- and velocity-dependent damping coefficient. The correlations between the structure of the water lubricant film and its frictional properties are found in a wide range of applied loads and for various strengths of interactions between water and surfaces. A self-organization of the film into a low-friction state under driving is observed to occur. Surprisingly, it is found that the "hydrophilic" surfaces exhibit a lower friction than the "hydrophobic" ones. The viscosity of the confined water estimated from the simulations is in a good agreement with the experimental value.

KEY WORDS: nanotribology, boundary lubrication friction, dynamic modelling, friction mechanisms, static friction, stick–slip
PACS numbers: 46.55.+d81.40.Pq

1. Introduction

Water adsorbed on solid surfaces is omnipresent. It almost always contaminates contact areas between solid bodies in natural or industrial environment, where it usually comes from the atmosphere [1]. As is well known from everyday experience, wet surfaces are very slippery and, thus, dangerous for car traffic especially when temperature is close to 0 °C. Lubrication properties of water had been known already from ancient times, when Egyptians (2400 BC) used water to lubricate wooden sledges to transport large stones to build the pyramids. Moreover, nature selected water as a base for the biological lubricants, that are far superior to the man-made oil-based lubricants [2]. However, water itself did not attract, until recently, much attention as a lubricant in man-made devices, due to two reasons: first, many surfaces undergo corrosion in the presence of water, and second, the water may be squeezed out from the contact area due to its very low viscosity. However, both of these problems could be resolved by a proper choice of surfaces coated for protection against corrosion and by use of hydrophilic surfaces to avoid squeezing out the water. It seems surprising therefore, that in spite of all this importance of water in tribology, the problem of friction of a thin water layer between two substrates in moving contact has not been explored in detail until now.

*To whom correspondence should be addressed.
E-mail: mpaliy@uwo.ca

Understanding of the role of water in friction as well as of the effect of the nature of surfaces involves knowledge of the phase behaviour of water under confinement. Even in the bulk, the phase diagram of water is quite intricate around the freezing point, where water demonstrates anomalies related to the hydrogen bonding between its molecules [3]. Its behavior can be dramatically different in a confined geometry, i.e. in a thin nanoscale layer. Both experiments [4,5] and computer simulations [6–8] of thin layers of water reveal the transitions between various liquid, amorphous and crystalline phases of water and ice not found in the bulk.

Our aim in the present article is to explore how the complex phase portrait of the confined water can manifest itself in its dynamics, namely *in the frictional properties* of a thin water film, when the confining surfaces move relative to each other. As we will show, water indeed can operate as a quite good and cheap lubricant.

2. Model

To study a thin film of water confined between two flat substrates, we use Molecular Dynamics (MD) technique based on Langevin equations with coordinate- and velocity-dependent damping coefficient [9]. Each of the substrates is made of two layers of $N_{\mathrm{sub}} = 24 \times 11$ atoms organized into lattices of square symmetry with

the lattice constants $a_x = a_y = 2.5$ Å. The outmost substrate layers are rigid, while the atoms belonging to the layers in the immediate contact with the lubricant are allowed to move in three spacial directions. The outmost layer of the bottom substrate is kept fixed, while the outmost layer of the top substrate is driven by a stage with a velocity v_s through an attached spring of elastic constant $k_s = 10^{-3}$ eV/Å^2 per atom. Between the substrates we put $N_{H_2O} = 336$ water molecules as shown in figure 1. In the x and y directions we apply periodic boundary conditions.

For the interactions in water, we use the *central-force* (CF) model due to Lemberg, Stillinger and Rahman [10] with refinements to correct the hydrostatic pressure [11], which yields a quite reliable description of water. In the CF model, the pair interactions between all oxygen and hydrogen atoms have the following form:

$$V_{ij}(r) = rA_{ij}^{(1)}/ + A_{ij}^{(2)}/r^{\beta_{ij}^{(2)}} + A_{ij}^{(3)}\left[1 + e^{\gamma_{ij}^{(3)}(r-\rho_{ij}^{(3)})}\right]^{-1} + A_{ij}^{(4)}\left[1 + e^{\gamma_{ij}^{(4)}(r-\rho_{ij}^{(4)})}\right]^{-1} + A_{ij}^{(5)}e^{-\delta_{ij}^{(5)}(r-\rho_{ij}^{(5)})^2}$$

where the index ij is equal to OO, OH or HH for the corresponding atomic pair, and the values of all coefficients in equation 1 are taken from Ref. [11]. The long-range Coulombic part of the interaction is handled via 3D Ewald summation with z-dipole correction for the slab geometry [12]. The size of the system in the z direction is taken as $L_z = 60$ Å, compared to a typical slab thickness of 10–13 Å and the box sizes in the periodic directions $L_x = 60$ Å and $L_y = 27.5$ Å. We use the Ewald parameter $r_E = 3.33$ Å, whereas the reciprocal space sum has been cut off at the distance 1.13 Å^{-1}, which includes 1274 wavevectors into the summation. All short range interactions in the model are smoothly truncated at $r_c = 10$ Å.

The substrate atoms interact with the water and between themselves via generalized Lennard–Jones (LJ) potential

$$V_{ij}(r) = \left[V_{ij}^{(0)}/(\mu - \nu)\right]\left[\nu\left(r_{ij}^{(0)}/r\right)^{\mu} - \mu\left(r_{ij}^{(0)}/r\right)^{\nu}\right].$$

For the interaction between the substrate atoms (denoted as S) the parameters are $\mu = 8$, $\nu = 4$, $V_{SS}^{(0)} = 1$ eV and

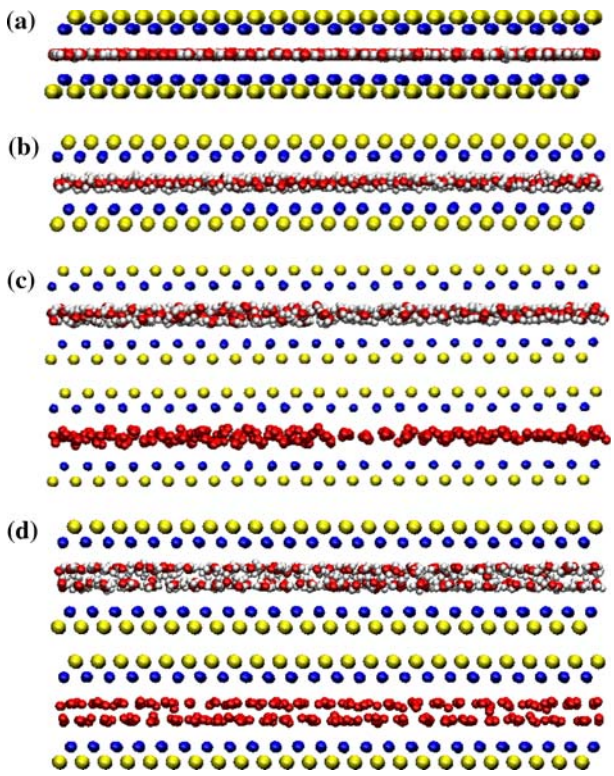

Figure 1. (color online): The model of the confined water film. Red/gray spheres show the oxygen/hydrogen atomic sites in the water molecules, while yellow and blue spheres depict the atomic sites of the outer (rigid) and inner (flexible) substrate layers, respectively. The load and shear are applied to the rigid part of the top substrate. The rigid part of the bottom substrate is fixed. The panels (a)–(d) demonstrate the structures of the water lubricant film that correspond to different values of the load f_l and the water–substrate interaction V_{SO}. (a) The completely flat one-layer structure observed at high loads $f_l = 1 - -10$ eV/Å (the concrete value of f_l depends on the water–substrate interaction V_{SO}). (b) The flat structure of oxygen atoms with protruding hydrogen atoms observed at moderately high loads and water–substrate interactions. (c) The "buckled" one-layer structure of oxygen atoms observed at intermediate loads and intermediate water-substrate interactions (the bottom figure shows the same configuration without hydrogen atoms depicted). (d) The two-layer structure (either liquid or solidified) observed at lower loads and lower values of the substrate–water interaction.

$r_{SS}^{(0)}$ = 2.5 Å. For the interactions between the substrate and water we took $\mu = 12$ and $\nu = 6$, and the parameters for the substrate–oxygen and substrate–hydrogen interaction are r_{SO} = 3.55 Å, r_{SH} = 3.19 Å and V_{SH} = 0.5 V_{SO}, which describe approximately the van der Waals interaction between a water molecule and a quartz (SiO_2) surface [7]. The value of V_{SO} was varied from 0 up to 0.25 eV which is a value of the order of the hydrogen bonding interaction between water molecules. In friction studies we mainly use two values for the water–substrate interaction: a relatively strong interaction V_{SO} = 0.05 eV which we interpret as the "hydrophilic" surface, and a very small interaction V_{SO} = 0.0025 eV which corresponds to the "hydrophobic" surface.

The atomic masses were taken as m_O = 16 amu and m_H = 1 amu, and for the atoms of the substrates, the silicon atom mass $m_S = 28.1$ amu. The equations of motions were integrated using the velocity–Verlet algorithm with the time step of 0.5 fs dictated by the CF model. The load force applied to the upper substrate was varied within the interval $f_l = 10^{-3}$–10 eV/Å per one substrate atom, which corresponds to the pressures $P = f_l/(a_x a_y) = 2.56 \times 10^{7-11}$ Pa. Note, however, that even the corrected CF model still overestimates the normal pressure of 1 Bar in about 100 times [11], so that the use of even higher pressures in simulation could be considered as reasonable ones.

The coordinate- and velocity-dependent damping coefficient $\eta(z,v)$ in Langevin equations has been designed to mimic a realistic situation, as described in detail in Ref. [9]. Here we sketch only its main features: (i) the damping $\eta(z,v) = \eta_1(z)\eta_2(v)$ exponentially decays away from the substrates as $\eta_1(z) = 1 - \tanh[(z - a^*)/a^*]$, where a^* = 3 Å is a characteristic distance of the order of lattice spacing; (ii) its velocity dependence $\eta_2(v) = \eta_{min} + \eta_{ph}(\omega_{wash})$, where $\omega_{wash}(v) = 2\pi v/a^*$ is the *washboard frequency* of driving, includes a frequency-dependent phonon term $\eta_{ph}(\omega)$ vanishing beyond a cut-off (Debye) frequency of the substrate $\omega^* \approx 65.5\,\mathrm{ps}^{-1}$, and an additional damping η_{min} due to multiphonon processes and the creation of electron-hole pairs in the substrate. In our simulations we used a reasonable estimate for an adsorbed atom [13], $\eta_{min} = 0.01\omega_s$, where $\omega_s = \left[V''_{SS}(r_{SS})/m_S\right]^{1/2} \approx 41.9\,\mathrm{ps}^{-1}$ is a characteristic frequency of the substrate.

Finally, initial configurations were prepared from disordered high-temperature configurations by annealing with the temperature slowly decreasing towards T = 300 K. This results in a liquid or amorphous-ice film as a typical initial state.

3. Structure of the confined water film

We begin with the study of the equilibrium structure of the confined film as it changes with variation of the applied pressure f_l and the water–substrate interaction V_{SO}.

The MD runs proceed as follows. We start from the lowest value of the load force $f_l = 10^{-3}$ eV/Å and anneal the system at T = 300 K during time period of 20 ps, and then, also during 20 ps, we measure the total potential energy of the system and the position of the top substrate z which characterizes the thickness of the lubricant film. We checked that this time is sufficient for our system to reach the equilibrium. Then we increase the applied load by the logarithmically equidistant steps up to the maximum value $f_l = 10$ eV/Å, repeating at every step the measurements described above. After that, the whole procedure is repeated during the decrease of the load back to $f_l = 10^{-3}$ eV/Å.

The simulation results showed that on the decompression, the film is always thinner than during the compression process. The relative stability of the film structure can be estimated by the value of the total potential energy. We found that if the interaction of the water with the substrates is high enough, $V_{SO} \gtrsim 0.1$ eV, the system state during the decompression process is energetically preferred over the "uncompressed" one. This can be explained by the following argument: When the water film is more compressed, then more oxygen and hydrogen atoms interact simultaneously with both (top and bottom) substrates via the attractive part of the LJ potential. Therefore, if V_{SO} is high enough, this attraction results in the net decrease of the overall energy of the system, compared to the uncompressed state, even in spite of the increase of energy due to the repulsive core interaction between the H and O atoms because of compression of the water layer.

Visual inspection of the atomic configurations suggests that the film can exist in several distinct states, or phases. At lower loads f_l and water–substrate interactions V_{SO} the water film is always in the two-layer liquid state, which solidifies with the increase of the load (figure 1(d)). With the further increase of the applied load, the film is transformed finally to a completely flat state (figure 1(a)), where all O and H atoms are situated in one layer and all water molecules have in-plane orientation. In between these extreme cases, depending on the load and the magnitude of the interaction with the substrates, the water film can exist in two other states. One of them, which is observed at higher loads, is characterized by flat in-plane structure of oxygen atoms, while the hydrogen atoms are protruded to both sides of the film (figure 1(b)). Another structure of the film is the "buckled" structure, where the oxygen atoms form a buckled layer, and hydrogen atoms are again protruding on both sides of the film (figure 1(c)). The buckling of the very thin water film has earlier been observed in numerical experiments of the layer confined between two substrates with the change of the distance between the substrates at a fixed pressure [7]. The buckling emerges, because the out-of-plane positions of the oxygen atoms in the buckled monolayer help to minimize

the distortions of the hydrogen bonds. The complete phase diagram of the water confined between the flat surfaces has recently been calculated within the help of the TIP4P model of water, and the place of the buckled "monolayer ice" phase in the diagram has been located [14]. Although we use a different model (the CF model with atomically corrugated walls and the fixed number of water molecules), we observe similar transitions to/from the buckled ice structure with the change of pressure. The buckled phase is observed in between two other ice structures, the flat one- and two-layer ice phases.

4. Static and kinetic friction forces

In friction experiments, we slowly increase the driving velocity v_s starting from zero to a given value, keeping the temperature at $T = 300$ K. Typical dependences of the spring force f (per one substrate atom) on time are presented in figure 2. When the stage moves with a low velocity ($v_s = 0.3$ Å/ps = 30 m/s), the spring elongates and the force increases linearly with time until it reaches the value of the static friction force ($f_s \approx 0.03$–0.04 eV/Å). At this moment the top substrate begins to slide and catches up with the stage, so that f decreases, the substrates stick again, and the whole cycle is repeated. This is the *stick–slip* regime shown in Figs. 2(a) and (b). At a higher stage velocity ($v_s = 3$ Å/ps = 300 m/s), the *smooth sliding* is observed, Figs. 2(c) and (d), and the spring force is equal to the kinetic friction force f_k.

Let us first present the simulation results for the "hydrophilic" surface, $V_{SO} = 0.05$ eV. At this V_{SO} value, the "uncompressed" configuration of the water film obtained during the compression process, is more stable with respect to the "compressed" configuration.

Starting from the configurations obtained during the compression/decompression runs described above, we measured both static f_s and kinetic f_k friction forces as functions of the applied load fl.The results are presented in figure 3, where solid symbols and curves are for the friction forces obtained from the "uncompressed" (more stable) configurations, while open symbols and dotted curves, for the ones obtained from the "compressed" (metastable) initial configurations.

First, the static and kinetic frictional forces stay approximately constant up to the load $f_l \sim 0.1$ eV/Å, both for the "uncompressed" and "compressed" initial configurations. Therefore, the "tribological" friction coefficients $\mu = f_{s,k}/f_l$ strongly decrease with the load. For the "uncompressed" configurations (solid symbols and curves in figure 3), the structure of the film always corresponds to two layers, up to the load $f_l \approx 0.1$ eV/Å. The lubricant film is always solidified, as it is attested by nonzero values of the static friction force $f_s \approx 0.02$–0.03 eV/Å. During slips in the stick–slip regime at lower driving velocities, the film does not melt, and it advances approximately half the distance travelled by the top substrate. Thus, the stick–slip is governed by inertia effects. At higher driving velocities the system exhibits smooth sliding. At a lower load, $f_l = 10^{-3}$ eV/Å, the smooth motion corresponds to the "layer-over-layer" sliding, accompanied by noticeable diffusion of water molecules between the lubricant layers. At higher f_l values, the lubricant remains solid during sliding, and the film moves as a whole. In both cases the sliding is *symmetric*, the film in average moves with the half of the top substrate velocity, $v_{film} \approx v_s/2$, and the kinetic friction force $f_k \approx 0.02$ eV/Å is approximately equal to the static one.

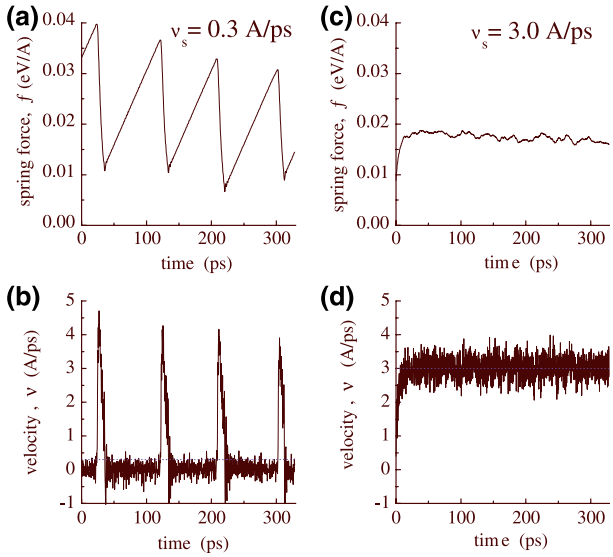

Figure 2. Typical time dependences of the spring force [panels (a) and (c)] and the velocity of the upper substrate [panels (b) and (d)] for the regimes of stick–slip motion [panels (a) and (b)] and smooth sliding [panels (c) and (d)]. The values of the driving velocity are $v_s = 0.3$ Å/ps [(a) and (b)] and 3 Å/ps [(c) and (d)]. The parameters are $V_{SO} = 0.05$ eV and $f_l = 1$ eV/Å.

The structure and frictional behavior of the "compressed" configurations (open symbols and dotted curves in figure 3) are different. At the low loads $f_l < 0.1$ eV/Å, the lubricant film always has the "buckled one-layer" structure (figure 1(c)), which is metastable with respect to the two-layer "uncompressed" configuration. It also shows stick–slip motion at lower driving velocities and smooth sliding at higher driving velocities, with approximately two times higher values of both static and kinetic friction forces as compared with those for the "uncompressed" initial configurations. Now, however, the kinetic friction force ($f_k \approx 0.033$ eV/Å) is smaller than the static one ($f_s \approx 0.045$ eV/Å). An important difference from the "uncompressed" case is that now the sliding is *asymmetric* both during the slips in the stick–slip regime and in the smooth sliding regime. The water film moves being attached to one of the substrates. The increase of both the static and kinetic friction forces for the "compressed" configurations as compared to the "uncompressed" ones can be explained in the following way. Let us consider the number of bonds participating in the interaction of the film with the substrates. While in the two-layer "uncompressed" film, only half of water molecules interact with a substrate, this fraction is much larger than 0.5 (and approaches 1) for the film in the (buckled) one layer configuration. Therefore, when the film moves, the rate of the breaking/forming of these bonds is much higher for the case of the "compressed" film, resulting in the increase of the friction forces.

Now let us describe the friction properties at high loads $f_l > 0.1$ eV/Å. As one can see from figure 2, the static friction force decreases directly in the course of the stick–slip motion. This decrease is associated with the structural transition in the driven lubricant film. Namely, let initially the film had the "buckled structure" as that of figure 1(c), which is characterized by a high static friction force $f_s \approx 0.09$ eV/Å. However, already after the first slip, the film restructures itself towards a flatter, more "compressed" structure, which is characterized by much lower value of the static friction force $f_s \approx 0.03$ eV/Å (such decrease of the friction force is denoted with the "error bars" in figure 3). Note that the tendency of the lubricant film to self-organize into a

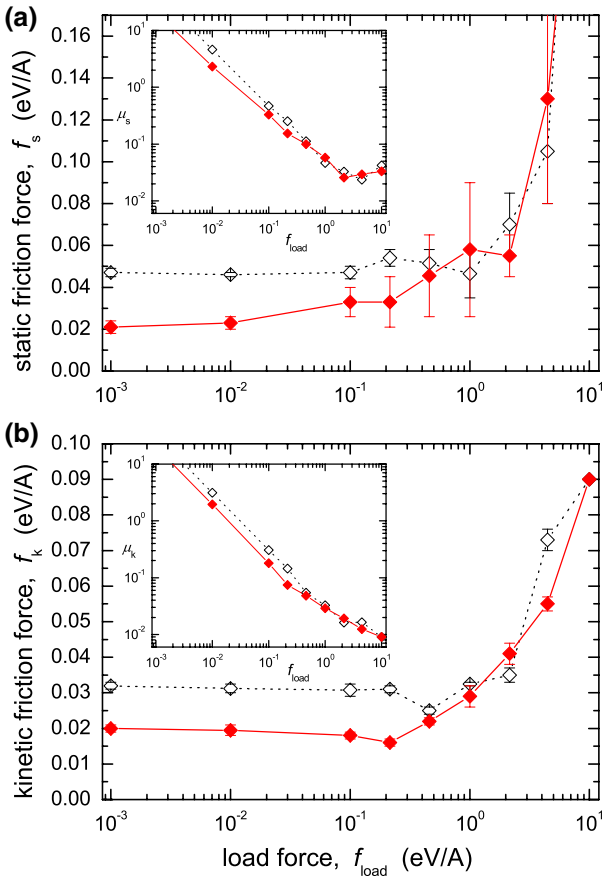

Figure 3. (color online): (a) The static friction force f_s versus the applied load f_l for the hydrophilic surfaces, $V_{SO} = 0.05$ eV. Solid symbols and curve indicate the friction force obtained from the "uncompressed" (more stable) configurations, while open symbols and dotted curve denote the friction force obtained from the "compressed" (metastable) ones. The highest/lowest values of the friction force found in the simulation runs are denoted with "error bars". Inset shows the "tribological" friction $\mu_s = f_s/f_l$. (b) The same for the kinetic friction f_k at the driving velocity $v_s = 3$ Å/ps.

low-friction phase has also been observed in a simple system of Lennard–Jones atoms [15] as well as in a more realistic MD simulation of a dodecane film confined between mica surfaces [16].

At the high loads, $f_l \gg 0.1$ eV/Å, the friction forces grow with the load. The static coefficient $\mu_s = f_s/f_l$ achieves a plateau $\mu_s \approx 0.03$ in this case (in agreement with Amontons' law), while the kinetic coefficient $\mu_k = f_k/f_s$ continues to decrease with load growing.

Next, let us consider the case of the "hydrophobic" surfaces with the water–substrate interaction $V_{SO} = 0.0025$ eV, and repeat the simulations as described above at two values of the load force, $f_l = 0.46$ eV/Å and $f_l = 1$ eV/Å, in both cases starting from the "uncompressed" configurations of the lubricant film.

While the overall behavior during these runs is the same as described above (stick–slip motion with a transition to smaller values of the static friction force at lower driving velocities, and smooth sliding at higher driving velocities), the values of both friction forces are systematically higher in the case of the "hydrophobic" walls. The increase in friction is moderate at the smaller load $f_l = 0.46$ eV/Å, where we found $f_s \approx 0.05$–0.09 eV/Å and $f_k \approx 0.04$ eV/Å for the "hydrophobic" system as compared with the forces $f_s \approx 0.02$–0.06 eV/Å and $f_k \approx 0.025$ eV/Å for the "hydrophilic" system (figure 3). However, the effect is much more pronounced at the high load $f_l = 1$ eV/Å: now we obtained the values $f_s \approx 0.1$–0.17 eV/Å and $f_k \approx 0.1$ eV/Å, i.e., 3-fold increase of the friction for the "hydrophobic" system comparing with the "hydrophilic" one, where $f_s \approx 0.03$–0.09 eV/Å and $f_k \approx 0.03$ eV/Å (figure 3).

A reason for such behavior can be rationalized from the inspection of atomic configurations. Typical snapshots during smooth sliding under the load $f_l = 1$ eV/Å are shown in figure 4(a) for "hydrophilic" surfaces and figure 4(b) for "hydrophobic" surfaces. In the "hydrophilic" case, figure 4(a), the water molecules form during sliding almost purely *flat* triangular structure, while in the "hydrophobic case", figure 4(b), more water molecules are protruding towards the substrates from both upper and lower surfaces of the lubricant layer, thus forming the point-like defects. This is the consequence of the much weaker interaction of the water molecules with the substrate atoms, so that the "hydrophobic" surface cannot impose its flat structure on the water layer, contrary to the situation observed for the "hydrophilic" surface. Namely a *rougher morphology* of the water layer in contact with the "hydrophobic" surfaces results in the increase of both static and kinetic friction in this case.

It is interesting to point out that in the case of "hydrophilic" surfaces, figure 4(a), the water molecules form the triangular structure, which is weakly *commensurate* with the structure of the substrates. Namely, in the y direction (perpendicular to the driving), the commensurability is perfect (the water molecules are arranged with the same lattice constant as the substrate atoms), while in the x direction (direction of the driving) we found that every 15 rows of water molecules are placed approximately within the length of 12 substrate lattice constants, so that the 24×11 substrate lattice can almost perfectly accommodate 336 water molecules, from which $30 \times 11 = 330$ molecules form a perfect structure, while the remaining 6 water molecules are accommodated as in-plane extended dislocation-like defects, and the layer structure remains flat.

In the case of the "hydrophobic" surfaces, the structure of the water layer is also triangular, but now it is (almost) *incommensurate* with the substrates. This also is the consequence of the much weaker interaction of the water molecules with the substrate atoms, so that the "hydrophobic" surface cannot impose its structure on the water layer, contrary to the situation observed for the "hydrophilic" surface. As is well known, an incommensurate structure at the interface should result in much smaller friction, thus the "hydrophobic" surface has to exhibit lower values of f_s and f_k contrary to what we observed in simulation. However, the effect of roughness of the water layer in contact with the "hydrophobic" surfaces is stronger than the incommensurability effects, thus resulting in the increase of friction in "hydrophobic" systems.

Thus, we come to a surprising counter-intuitive conclusion: a *stronger* attractive interaction of the water with the substrates results in *smaller* both static and kinetic friction forces, i.e. more "hydrophilic" substrates lead to decreased friction.

In the simulations presented above we used fixed number of water molecules, which may lead to undesired artifacts in our system with periodic boundary conditions. To check this point, we also repeated the sliding experiments at different numbers of water molecules in the lubricant layer, $N_{H_2O} = 294$, 315, 336, 357, 378, 399, and 420. The results showed that the static and kinetic friction forces change in antiphase: while the

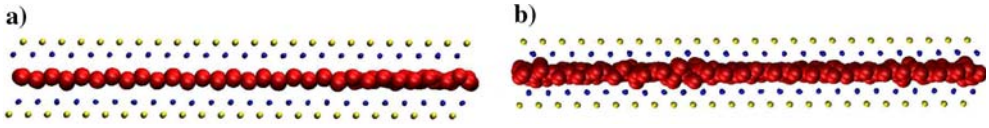

Figure 4. (color online): Side views of the atomic configurations during smooth sliding ($v_s = 3$ Å/ps) for the cases of "hydrophilic" (a) and "hydrophobic" (b) surfaces.

static friction force f_s grows monotonically with N_{H_2O}, the kinetic friction force f_k demonstrates an overall decrease with N_{H_2O}. However, all conclusions reached above remain unchanged.

Now let us compare our results with those available from other simulations and experiments. For the flat geometry, the frictional force per unit area is $F_x/A = -\sum_\alpha \sigma'_{x\alpha}\delta_{\alpha z}$, where $\alpha = x, y, z$, A is the total area of the surfaces in contact, and the stress tensor in the linear approximation for uncompressed liquid is determined by the *viscosity coefficient* $\tilde{\eta}$,

$$\sigma'_{\alpha\beta} = \tilde{\eta}\left(\frac{\partial v_\alpha}{\partial x_\beta} + \frac{\partial v_\beta}{\partial x_\alpha}\right).$$

Thus, the total kinetic frictional force is $F = -A\sigma'_{xz} = -A\tilde{\eta}\partial v_x/\partial z \approx -A\tilde{\eta}v_{top}/d$, where d is the width of the lubricant film and $F = -fN_{sub}$, so that we finally obtain

$$\tilde{\eta} = fd/v_{top}a_x a_y.$$

The experimental value for the viscosity coefficient of the bulk water is known to be $\tilde{\eta} \approx 10^{-3}$ kg/(m s). Even though we have not calculated directly this property for the modified CF water model used, we may estimate, using the Stokes–Einstein relation and the known experimental and CF model values for the diffusion coefficient in the bulk [17], that the CF model overestimates only slightly (~1.6 times) the viscosity coefficient of the bulk water. At the same time, in our simulation of the confined water layer for smooth sliding with the velocity $v_s = 3$ Å/ps we found that $d \approx 10$ Å and $f \gtrsim 0.02$ eV/Å, which corresponds to the "hydrodynamic" viscosity coefficient $\tilde{\eta} \gtrsim 1.7 \times 10^{-3}$ kg/(m s), i.e. one obtains about the same value of $\tilde{\eta}$ as expected for the bulk.

One has to note that, unfortunately, only very high shear rates 10^8–10^{12} s^{-1} are currently accessible in MD simulations (even though some attempts to circumvent this problem have been made recently [18]). These rates are 7–9 orders of magnitude higher than those used in the experiments [19]. Such rapid shear may result in so-called "shear thinning" effect, i.e. in the decrease of the viscosity of the film, as illustrated e.g. in a recent simulation by Leng and Cummings of thin water layers confined between two mica plates [20]. The authors of Ref. [20] observed that for the thinnest water layer they studied (~0.9 nm) the viscosity is very high (~80 times the bulk value) at low shear rates, whereas a strong decrease of the viscosity down to the bulk value occurs at the shear rates higher than $10^9 s^{-1}$ (the authors associate this effect with the rotational correlation time for the water dipoles). At the same time, for the thicker layers (1.65 and 2.4 nm) almost no shear thinning is observed in Ref. [20], and the viscosity is found to be comparable to the bulk value at all shear rates studied. It is difficult to directly compare our results with those of Leng and Cummings, mainly because of the presence of large solvated K^+ ions, bound to the surfaces, in their system. In particular, two layers of K^+ ions must already account for most of the width of the thinnest layer they studied (figure 1 of Ref. [20]), so that there seems to be virtually no intermediate water in between, and the shear dynamics should be very different from that found for the thicker layers. However, the results of Ref. [20] for the thicker layers can be better compared with our results (in our system we have always at least 1.5 uncompressed water layers between the substrates). Such comparison (corroborated also by the data drawn from figure 4 of Ref. [18]) allows us to predict that the possible decrease of the viscosity due to the shear thinning effect in our system should not be stronger than ~2 times or so. Thus we obtain a very good agreement with experiments on the viscosity of water film confined between two mica plates with a thickness about 1–2 molecular layers, where the values within a factor of 3 or so of the viscosity of bulk water were observed [19]. The values of the coefficient of friction $\mu = f/f_l \sim 0.01$ that we obtained in simulations at high loads, also lie in the range of experimentally observed values [21].

5. Conclusion

In the present paper we reported the detailed MD study of the friction properties of the ultrathin water film confined between two solid surfaces in moving contact. With the increase of the load, the film is solidified (at room temperature) passing through two ice-like structures and taking finally a completely flat configuration. The viscosity of the thin water film takes values within a factor of $\gtrsim 2$ of the viscosity of bulk water, which is in good agreement with available experimental data. The complex phase portrait of the confined water manifests itself into its frictional properties. We found numerous and specific for water correlations between the lubricant structure and the changes in both static and kinetic friction forces. Besides, we observed the transition from the high- to low-friction phases of the water film directly in the course of the stick–slip motion, which emerges due to self-organization of the lubricant film.

The system demonstrates the transition from stick–slip to smooth sliding at an atomic-scale velocity of the order $v_c \sim 1$ Å/ps = 100 m/s. The film remains solidified during slips; therefore the stick–slip motion is governed by inertia effects contrary to the melting/freezing mechanism of oil-like lubricants. The film may be melted due to driving, but this occurs at a quite high driving velocity $v > 10$ Å/ps. Note that such features are similar to those observed for simple Lennard–Jones lubricants [9, 22, 23].

Amontons' law (which states that the ratio $\mu = f/f_l$ is approximately constant) operates only for the static

friction coefficient and only at high loads $f_l > 1$ eV/Å, where it reaches a value $\mu_s \approx 0.03$. The kinetic friction coefficient monotonically decreases with the load and takes relatively low values $\mu_k \sim 0.01$ and even lower at high loads. Thus, the water film can operate as a quite good lubricant for surfaces which are protected from corrosion.

However, an important question is about squeezing of the water film out of the contact area at the high load. If the water will be squeezed out so that the surfaces will come to a direct contact, this may result in their wearing or damaging. This question needs further investigation. In this context we note, however, that squeezing is less expected to occur for hydrophilic surfaces, when the water is strongly adhered to the surface. Surprisingly, we found that the hydrophilic surfaces demonstrate much better friction properties than hydrophobic surfaces.

M.P. and S.C. thank NSERC and Premier's Research Excellence Award for support, and Canadian Foundation for Innovation (CFI) for the grant used to build computer facilities employed in this work. Chemical Physics Theory Group at the University of Toronto is gratefully acknowledged for kindly providing their CFI/OIT-funded cluster, where part of the calculations has been done. O.B. was partially supported by the Ministry of Ukraine for Education and Science (Project No. F7/279-2001). M.P. thanks A. Zhukov for useful discussions.

References

[1] B.N.J. Persson, *Sliding Friction* (Springer-Verlag, Berlin, 1998); Surf. Sci. Rep. 33 (1999) 83.
[2] M. Urbakh, J. Klafter, D. Gourdon and J. Israelachvili, Nature 430 (2004) 525.
[3] V.F. Petrenko and R.W. Whitworth, in: *Physics of Ice* (Oxford University Press, Oxford, 1999); H.E. Stanley, Mater. Res. Bull. 24 (1999) 22; H.E. Stanley *et al*, J. Phys. Condens. Matter 12 (2000) 403.
[4] J.D. Porter and A.S. Zinn-Warner, Phys. Rev. Lett. 73 (1994) 2879.
[5] R. Bergman and J. Swenson, Nature 403 (2000) 283.
[6] M. Meyer and H.E. Stanley, J. Phys. Chem. 103 (1999) 9728.
[7] R. Zangi and A.E. Mark, Phys. Rev. Lett. 91 (2003) 025502; J. Chem. Phys. 119 (2003) 1694.
[8] J. Slovak *et al*, Physica A 319, (2003) 163; K. Koga, H. Tanaka and X.C. Zeng, Nature 408, (2000) 564; K. Koga, X.C. Zeng and H. Tanaka, Phys. Rev. Lett. 79 (1997) 5262.
[9] O.M. Braun and M. Peyrard, Phys. Rev. E 63 (2001) 046110; O.M. Braun and R. Ferrando, Phys. Rev. E 65 (2002) 061107.
[10] H.L. Lemberg and F.H. Stillinger, J. Chem. Phys. 62, (1975) 1677; F.H. Stillinger and A. Rahman, *ibid*. 68 (1978) 666.
[11] D.-M. Duh, D.N. Perera and D.J. Haymet, J. Chem. Phys. 102 (1995) 3736.
[12] I.-C. Yeh and M.L. Berkowitz, J. Chem. Phys. 111 (1999) 3155.
[13] O.M. Braun, Surf. Sci. 213 (1989) 336.
[14] K. Koga and H. Tanaka, J. Chem. Phys. 122 (2005) 104711.
[15] O.M. Braun, M. Paliy and S. Consta, Phys. Rev. Lett. 92 (2004) 256103.
[16] A. Jabbarzadeh, P. Harrowell and R.I. Tanner, Phys. Rev. Lett. 94 (2005) 126103.
[17] F. Bresme, J. Chem. Phys. 115 (2001) 7564.
[18] J. Delhommelle and P.T. Cummings, Phys. Rev. B 72 (2005) 172201.
[19] U. Raviv, P. Laurat and J. Klein, Nature 413 (2001) 51; U. Raviv and J. Klein, Science 297 (2002) 1540.
[20] Y. Leng and P.T. Cummings, Phys. Rev. Lett. 94 (2005) 026101. The authors use fixed concentration of the TIP4P water molecules, at constant applied pressure 1 bar, and 298 K. The major difference from our simulations is the addition of the potassium ions K^+ that form bound hydration layers at both surfaces.
[21] A. Berman, C. Drummond and J. Israelachvili, Tribol. Lett. 4 (1998) 95.
[22] O.M. Braun, M. Peyrard, V. Bortolani, A. Franchini and A. Vanossi, Phys. Rev. E 72 (2005) 056116.
[23] O.M. Braun and A.G. Naumovets, Surf. Sci. Rep. 60 (2006) 79.